Self-organization of mammary epithelial lineages is driven by differential E-cadherin activity.

Lea Chanson[3]^, Douglas Brownfield[1,2]^, James C Garbe[1], Irene Kuhn[1], Martha R Stampfer[1], Mina J Bissell[1], and Mark A LaBarge[1]*

1: Life Sciences Division, Lawrence Berkeley National Laboratory, Berkeley, CA 94720
2: Department of Bioengineering, University of California, Berkeley, CA 94720
3: Institute of Bioengineering, Ecole Polytechnique Fédérale de Lausanne, CH-1015 Lausanne, Switzerland.
^: Authors contributed equally
*: Address correspondence to MALabarge@lbl.gov

Epithelial tissues in adults undergo remodeling and renewal in accordance with the ebb and flow of physiological demands. Thus a dynamic cohesive mechanism must exist that simultaneously fosters maintenance of organization and placement of new cells at appropriate locations as tissues are replenished and repaired. To determine whether adult epithelial cells innately possessed self-organization capabilities, we used a micropatterning approach to enforce a regular 3D geometry, combined with an algorithm to quantify changes of cellular distribution over time. Isogenic normal human mammary myoepithlial and luminal epithelial cells were shown to spontaneously self-organize into a configuration similar to their organization in vivo. Inhibition of adherens proteins and of the actomyosin network showed that the ability to form and remodel active cell-cell junctions impelled self-organization, rather than differential stiffness per se. We demonstrate that self-organization driven by lineage-specific differential E-cadherin activity is an innate property of mammary epithelial cells.

Most mammalian adult tissues are replenished and repaired throughout life by reservoirs of stem cells. As new somatic cells replace old ones or build new tissue, organization and architecture must be maintained. The alternative loss of organization in adult tissues is associated with cancer and other diseases. The robust ability to organize into tissues is marked from conception: heterogeneous aggregates of dissociated cells from embryonic tissues self-organize into semblances of the original tissues(*1-4*). The mechanisms governing self-organization during developmental morphogenesis(*5-8*) are likely conserved in the maintenance of organization in adult tissues. The human mammary gland undergoes monthly cycles of modest proliferation and involution, and the gland shows as much as a ten-fold expansion during

pregnancy followed by involution to normal size. During these processes, the precise bilayered branching organization throughout the gland is maintained; secretory luminal epithelial cells (LEPs) line the lumen, surrounded by a layer of contractile myoepithelial cells (MEPs) that are also adjacent to the basement membrane. We hypothesized that the various mammary epithelial cells possess lineage-specific intrinsic abilities to self-organize, which serves as one means to help maintain normal tissue architecture.

We first determined whether different lineages of cultured human mammary epithelial cells (HMEC), derived from reduction mammoplasty tissue, possessed an intrinsic ability to form bilayered structures. Subpopulations of LEPs and MEPs, defined as $CD227^{+}/CD10^{-}/K19^{+}/K14^{-}$ and $CD227^{-}/CD10^{+}/K19^{-}/K14^{+}$, respectively(*9*), were enriched from heterogeneous normal finite life-span HMEC(*10*) at passage 4 or 5 (Fig 1A-A''). The two populations were labeled with different wavelength long-term labeling fluorescent membrane dyes, mixed together, and suspended in hanging droplets. Over 48hrs we observed formation of LEP cores surrounded by MEPs (Fig 1B), similar to their organization in vivo. The considerable variation of aggregate size, shape, and focal planes obscured a quantitative understanding of the phenomenon, so we engineered a microwell assay that confined the HMEC mixtures to a 3D cylindrical geometry, which enabled quantification of lineage distributions over time (Fig 1C). Representative images at 0 and 48hrs of mixed LEPs and MEPs in microwells suggested self-organization had occurred, as compared to mixtures of arbitrarily labeled HMEC cultures (Fig 1D). Quantification of lineage distributions over time demonstrated that MEPs formed a ring surrounding clusters of LEPs in a majority of microwells as early as 24hrs (Fig 1E, top). Controls showed overlapping distributions of cells that did not resolve into distinct populations (Fig 1E, bottom). Thus self-organizing is an innate property of HMEC lineages.

Self-organizing behavior in tissues has been ascribed to disparate adhesive properties among the participating cells (the differential adhesion hypothesis (DAH), reviewed in(*5*)). Cadherin cell-cell adhesion molecules, particularly E-cadherin, play key roles in tissue morphogenesis during vertebrate gastrulation(*11*). Quantification of images of fluorescently immunostained tissue sections of normal mammary gland (Fig 2A) from two individuals revealed more E-cadherin protein present at the borders between two LEPs as compared to borders between a LEP and a MEP ($p<0.001$)(Fig 2B). Flow cytometer measurements of E-cadherin surface protein levels were made in LEPs and MEPs, as defined in Figure 1A. In HMEC strains from six individuals a reproducible pattern was observed, whereby more E-cadherin was detected on LEPs versus MEPs (Fig 2C). The lineage-specific expression levels of E-cadherin made it an attractive candidate for further testing of the DAH as it pertained to

organizing HMEC.

To determine whether cadherins played a functional role in self-organization of LEPs and MEPs, inhibitors of E-, P-, and VE-cadherin were added to the medium of the microwell assay to antagonize those specific cell-cell interactions. P-cadherin is expressed by MEPs in vivo, but not by LEPs(*12*). VE-cadherin is expressed by endothelial cells, not by epithelial cells(*11*), and was used as a control for potential effects of heterotypic cadherin interactions(*8*). An antibody that blocked E-cadherin, and recombinant E-cadherin fused to human IgG-Fc region (rEcad), prevented self-organizing of LEPs and MEPs (Fig 3A). An antibody that blocked P–cadherin, and recombinant VE-cadherin IgG-fusion protein (rVEcad), did not prevent organizing (Fig 3A). These data suggested that differential levels of E-cadherin at the surfaces of LEPs and MEPs were driving self-organization.

Compelling self-organization studies of dissociated cells from zebra fish embryos suggested that differential actomyosin-dependent cell-cortex tension directed cell sorting in those experiments(*7*). We therefore examined the impact on HMEC self-organization and stiffness of the actomyosin network inhibitors ML-7, a myosin light chain kinase (MLCK) inhibitor(*13*), and Y27632, a Rho kinase (ROCK) inhibitor(*14*). Both inhibitors prevented HMEC self-organization (Fig 3B). Atomic force microscopy was used to measure elasticity, also called stiffness. While untreated MEPs tended to be stiffer than LEPs, this difference was significant in presence of the inhibitors ($p<0.001$)(Fig 3C). MEPs stiffness was unaffected by ML-7 and Y27632, but they caused softening of the LEPs, (Fig 3C). That actomyosin network inhibitors increased the magnitude of the difference in elasticity between LEPs and MEPs, but did not alter their relative elasticity, suggested that self-organization was not caused by differential stiffness.

We thus investigated whether the actomyosin inhibitors affected expression or binding activities of E-cadherin in HMEC. Addition of ML-7 or Y27632 to the HMEC culture media did not change the lineage-specific differences in E-cadherin expression as measured via flow cytometry; invariably, LEPs expressed more E-cadherin than did MEPs (Fig 4A). The ability of rEcad simply to bind surfaces of HMEC in suspension was measured also by flow cytometry. Binding of rEcad did not occur in Ca^{2+}-free media or when HMEC were preincubated with E-cadherin blocking antibodies, as compared to rEcad added alone in normal media (Fig 4B). Y27632 did not prevent rEcad binding, and ML-7 had only a modest negative impact on binding (Fig 4B). Therefore, neither differential expression levels of E-cadherin, nor its ability to simply bind other E-cadherin molecules at the surface were impacted by ML-7 or Y27632.

We next considered the possibility that the actomyosin inhibitors modulated the ability of E-cadherin junctions to mature or to remodel(*15*), thus preventing HMEC organization. Unphosphorylated β-catenin associates with the cytoplasmic tail of E-cadherin and is necessary for establishing active E-cadherin junctions(*16*). Phospho-β-catenin levels were measured by phospo-flow cytometry in HMEC cultured in suspension in the presence of rEcad with and without actomyosin inhibitors. More of the phosphorylated form of β-catenin was seen in unstimulated MEPs than in LEPs (Fig 4C, top), consistent with lineage-specific E-cadherin expression levels. The LEPs in unstimulated and rEcad-stimulated conditions exhibited two closely juxtaposed peaks, corresponding to less and more phosphorylated forms of β-catenin, consistent with there being two pools, one associated with active junctions and the other cytoplasmic, respectively (Fig 4C, middle). ML-7 treatment with rEcad resulted in a shift to the phosphorylated form, indicating the E-cadherin junctions were unable to form (Fig 4C, middle). Treatment with Y27632 alone made little change compared to the unstimulated control. However, in presence of rEcad, Y27632 elicited a strong shift to the unphosphorylated form of β-catenin, suggesting that mature junctions in HMEC were unable to break down and recycle (Fig 4C, middle), a result previously observed in immortal cell lines(*17*). Parallel analysis of the MEPs revealed nearly identical findings, with exception that the unphosphorylated form of β-catenin was only observed in presence of rEcad, but not in unstimulated controls (Fig 4C, bottom). These data predicted that ML-7 would ablate already organized HMEC structures, whereas Y27632 would preserve them.

Accordingly, ML-7 or Y27632 were added to mixtures of LEPs and MEPs in the microwell assay, either just after adding cells into wells at 0hrs, or after 24hrs when the DMSO controls started to show signs of organizing (Fig 4D). When added at 0 hrs, both actomyosin network inhibitors prevented self-organization (Fig 4D). When added at 24hrs, ML-7 obliterated any hint of organization whereas Y27632 preserved the self-organized structures consisting of a LEP core encircled by MEPs (Fig 4D). Thus the actomyosin network exerted its effects on HMEC self-organization by modulating the maturation or the remodeling of E-cadherin junctions.

Self-organization of HMEC is driven by differential E-cadherin activity. In support of this view, a recent comprehensive literature review of intercellular adhesion and morphogenesis proposed that self-organizing is not simply due to differential levels of cadherin expression or of binding affinities, but that adhesion energy and the ability to remodel cell-cell junctions are crucial determinants(*19*). Here we have utilized normal finite life-span HMEC together with an

engineered organotypic culture system to quantify their innate self-organizing properties in isolation from a number of other confounding factors. Although we focused on cell-cell E-cadherin junctions, other adhesive and physical interactions are undoubtedly important in maintaining mammary gland organization and bear further dissection, such as desmosomal interactions between LEP and MEP(*18*). In HMEC we found that the stiffer MEPs sorted to the exterior. In contrast, studies using zebra fish indicated that the cell population with greater stiffness and overall tension sorted to the interior(*7*); differences between cell types, adherence, and morphology alter the assumptions one needs to derive the mechanical data, thus obscuring a direct comparison. However, cell-ECM interactions also will likely impact sorting in vivo because epithelial cells in contact with laminin-111, a principal component of basement membrane, become less stiff(*20*). Therefore, MEPs in vivo may be less stiff than LEPs due to their direct contact with basement membrane. Future iterations of organotypic models will need to take these interactions into consideration.

Studying self-organizing behavior of a human epithelium is challenging because results cannot be easily extrapolated to in vivo. However, observations of breast cancer pathogenesis suggest the basic mechanisms described herein are important for maintaining mammary gland organization. E-cadherin expression is frequently misregulated in breast cancers(*21, 22*), and a hallmark of the epithelial-to-mesenchymal transition, which is associated with invasive and aggressive breast cancer, is loss of E-cadherin(*23*). Finally, the mechanisms governing self-organization also are important in the context of regenerative tissue maintenance. As MEPs and LEPs are produced anew by mammary progenitor cells in vivo, they must adopt their appropriate place within the tissue, or alternatively, the progenitors must be able to move to experience instructive microenvironments that direct cell-fate decisions(*24*). Understanding tissue self-organization mechanisms may help to explain how stem cell differentiation and maintenance of tissue architecture in adults are coordinated.

Figure Legends

Figure 1 – Heterogeneous mixtures of luminal and myoepithelial cells spontaneously self-organize into ordered structures. (A) Flow cytometry analysis of fourth passage finite life-span human mammary epithelial cells (HMEC) reveals distinct populations of the two principal somatic epithelial lineages of mammary gland. Myoepithelial cells (MEPs), defined here as $CD227^-/CD10^+$, and luminal epithelial cells (LEPs), defined as $CD227^+/CD10^-$. (A' and A'') Immunofluorescence of sorted cells for MEP and LEP markers keratin (K)14 (red) and K19 (green), respectively, verified that (A') $CD227^+$ LEPs were $K14^-/K19^+$, and (A'') $CD10^+$ MEPs were $K14^+/K19^-$. Nuclei are counterstained with DAPI (blue). (B) Images of mixtures of fluorescently labeled LEPs (green) and MEPs (red) suspended in hanging droplets and imaged with a confocal microscope (B, left image) just after mixing at 0 hours and (B, right image) at 48 hours. Bar represents 20mm. (C) A cartoon representation of the microwell self-organization assay. Fluorescently labeled LEPs (green) and MEPs (red) were mixed together and added inside arrays of microwells that did not support cell adhesion. Thirty wells were imaged with a confocal microscope just after addition of cells at 0hrs and again at 24hrs and 48hrs. Fluorescence from both green and red channels in one optical section per well were binarized, then combined and averaged to generate two gray-scale composite images that were overlaid to generate a single two-color composite distribution map for each condition, where LEP distributions are represented in green and MEP distributions are red. (D) Representative fluorescence images of (D, top) LEP (green) and MEP (red) in four different microwells at 0hrs and 48hrs, and of (D, bottom) controls, which were heterogeneous HMEC arbitrarily labeled with red or green fluorescent label. (E) Distribution maps of (E, top) LEP (green) and MEP (red), or (E, bottom) control mixtures at 0hrs, 24hrs, and 48hrs time points.

Figure 2 – Epithelial lineages that comprise mammary gland differentially express E-cadherin. (A, left image) An image of a tissue section from a normal mammary gland, specimen XD01, embedded in paraffin and triple-immunostained to show expression of the MEP and LEP markers keratin (K)14 (red) and K19 (green), respectively, and (A, right image) E-cadherin (gray scale). Scale bars represent 20mm. (B) Dot plots show image quantification from two individuals, XD01 and XA01, of E-cadherin protein levels at the boarders between two LEP (K19+ LEP), between a LEP and a MEP cell (K14+ LEP), and background fluorescence as measured on stroma, which does not express E-cadherin (Stroma); n=100 for each cell type collected from at least three sections. (C) Flow cytometry analysis of E-cadherin expression in $CD10^+$ MEPs and $CD227^+$ LEPs in HMEC strains at 4^{th} or 5^{th} passage from six individuals. Both

image and flow cytometry analysis revealed that LEPs express more E-cadherin relative to MEPs.

Figure 3 – E-cadherin junctions and cytoskeleton regulatory molecules, ROCK and MLCK, are required for self-organizing. (A) Distribution maps showing the ability of E-, P-, or VE-cadherin blocking agents (anti-E-cadherin, recombinant (r)E-cadherin, anti-P-cadherin, or rVE-cadherin) to prevent self-organizing of LEP (green) and MEP (red). Only E-cadherin-specific agents impaired self-organization. (B) LEP (green) and MEP (red) distribution maps demonstrating the deleterious effects on self-organizing in presence of MLCK inhibitor, ML-7, or ROCK inhibitor, Y27632. (C) Atomic force microscopy measurements of LEP and MEP in presence of ML-7 and Y27632. The graph represents Elasticity (PKa), or stiffness, values for 45 cells per condition, interior line represents mean elasticity values, error bars show standard error.

Figure 4 – Self-organization among luminal and myoepthelial cells is driven by E-cadherin activity. (A) E-cadherin protein expression at the surface of LEPs and MEPs in presence of ML-7 or Y27632, as measured by flow cytometry. (B) Flow cytometry analysis of rE-cadherin binding to HMEC cell surfaces. (C, top) Phospho flow analysis of β-catenin phosphorylation in unstimulated LEP and MEP-enriched subpopulations. β-catenin phosphorylation in (C, center) LEPs and (C, bottom) MEPs in presence of ML-7 or Y27632 with and without rE-cadherin present. (D) LEP (green) and MEP (red) distribution maps showing the impact on self-organization over time (time points 0hrs, 24hrs, and 48hrs) when inhibitors ML7 and Y27632 were added at 0hrs or after 24hrs.

Acknowledgements

We thank Drs. James Nelson, Matthias Lutolf, and Celeste M Nelson for insightful discussions, CMN for providing micropatterned wafers, and Dr. Daniel Fletcher for use of his AFM. MAL is supported by National Institute on Aging, R00AG033176, and the National Cancer Institute, U54CA112970. MJB is supported by grants from the U.S. Department of Energy, Office of Biological and Environmental Research, a Distinguished Fellow Award to MJB and Low Dose Radiation Program (contract no. DE-AC02-05CH1123); by National Cancer Institute awards R37CA064786, U54CA126552, R01CA057621, U54CA112970 and U54CA143836; U01CA143233; by U.S. Department of Defense, W81XWH0810736. MRS and JCG are supported by Department of Defense grant BCRP BC060444 and U54CA112970.

1. M. S. Steinberg, *Science* **137**, 762 (Sep 7, 1962).
2. M. S. Steinberg, *Proc Natl Acad Sci U S A* **48**, 1769 (Oct, 1962).
3. M. S. Steinberg, *Proc Natl Acad Sci U S A* **48**, 1577 (Sep 15, 1962).
4. P. L. Townes, J. Holtfreter, *Journal of Experimental Zoology* **128**, 53 (1955).
5. R. A. Foty, M. S. Steinberg, *Int J Dev Biol* **48**, 397 (2004).
6. R. A. Foty, M. S. Steinberg, *Dev Biol* **278**, 255 (Feb 1, 2005).
7. M. Krieg *et al.*, *Nat Cell Biol* **10**, 429 (Apr, 2008).
8. Q. Shi, Y. H. Chien, D. Leckband, *J Biol Chem* **283**, 28454 (Oct 17, 2008).
9. R. Villadsen *et al.*, *J Cell Biol* **177**, 87 (Apr 9, 2007).
10. J. C. Garbe *et al.*, *Cancer Res* **69**, 7557 (Oct 1, 2009).
11. B. M. Gumbiner, *Nat Rev Mol Cell Biol* **6**, 622 (Aug, 2005).
12. Y. Shimoyama *et al.*, *Cancer Res* **49**, 2128 (Apr 15, 1989).
13. M. Makishima *et al.*, *FEBS Lett* **287**, 175 (Aug 5, 1991).
14. S. P. Davies, H. Reddy, M. Caivano, P. Cohen, *Biochem J* **351**, 95 (Oct 1, 2000).
15. M. Fukata, K. Kaibuchi, *Nat Rev Mol Cell Biol* **2**, 887 (Dec, 2001).
16. W. J. Nelson, *Biochem Soc Trans* **36**, 149 (Apr, 2008).
17. E. Sahai, C. J. Marshall, *Nat Cell Biol* **4**, 408 (Jun, 2002).
18. S. K. Runswick, M. J. O'Hare, L. Jones, C. H. Streuli, D. R. Garrod, *Nat Cell Biol* **3**, 823 (Sep, 2001).
19. N. Borghi, W. James Nelson, *Curr Top Dev Biol* **89**, 1 (2009).
20. J. Alcaraz *et al.*, *EMBO J* **27**, 2829 (Nov 5, 2008).
21. J. E. Korkola *et al.*, *Cancer Res* **63**, 7167 (Nov 1, 2003).
22. R. Moll, M. Mitze, U. H. Frixen, W. Birchmeier, *Am J Pathol* **143**, 1731 (Dec, 1993).
23. A. Cano *et al.*, *Nat Cell Biol* **2**, 76 (Feb, 2000).
24. M. A. LaBarge *et al.*, *Integrative Biology* **1**, 70 (January, 2009).

A

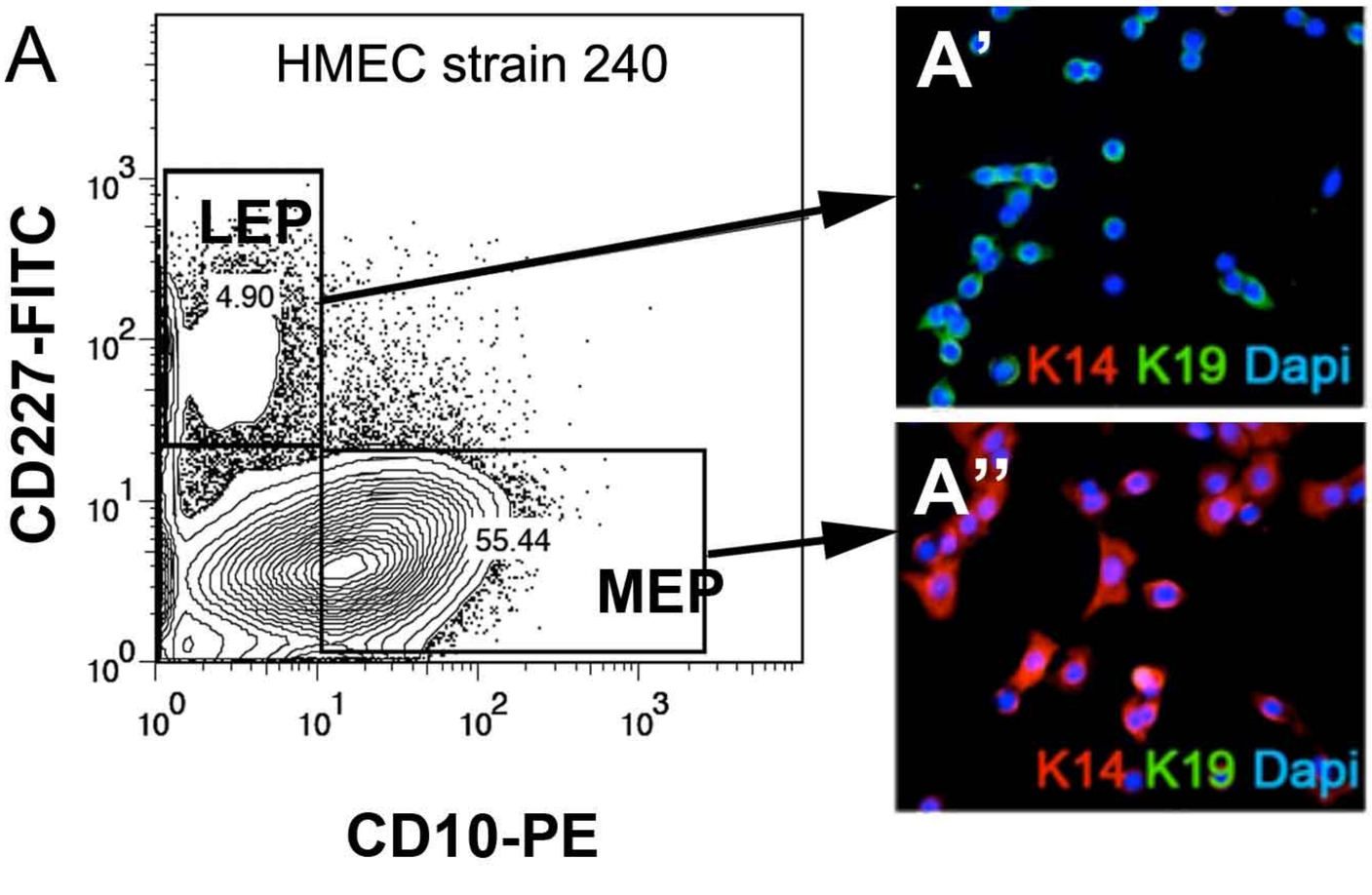
HMEC strain 240
LEP
4.90
MEP
55.44
CD227-FITC
CD10-PE
10^0
10^1
10^2
10^3

A'
K14 K19 Dapi
A''
K14 K19 Dapi

B

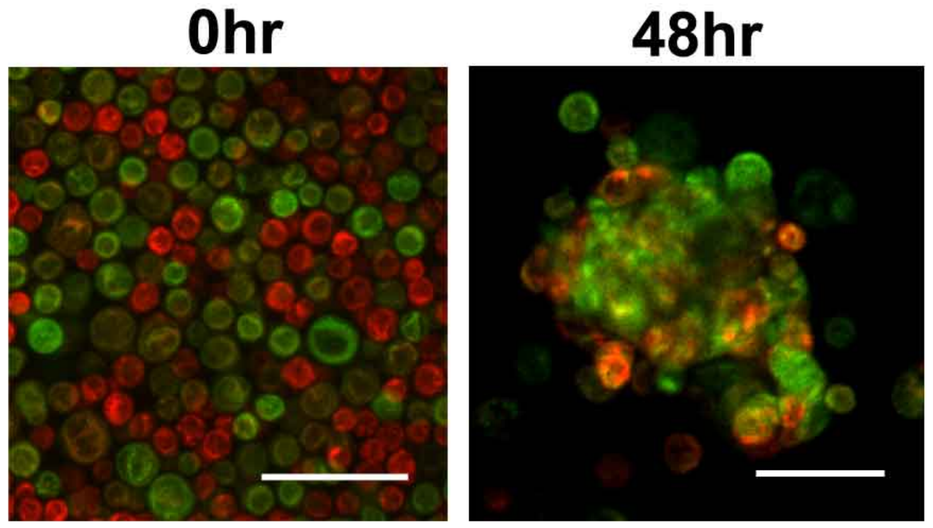
0hr
48hr
LEP
MEP

C

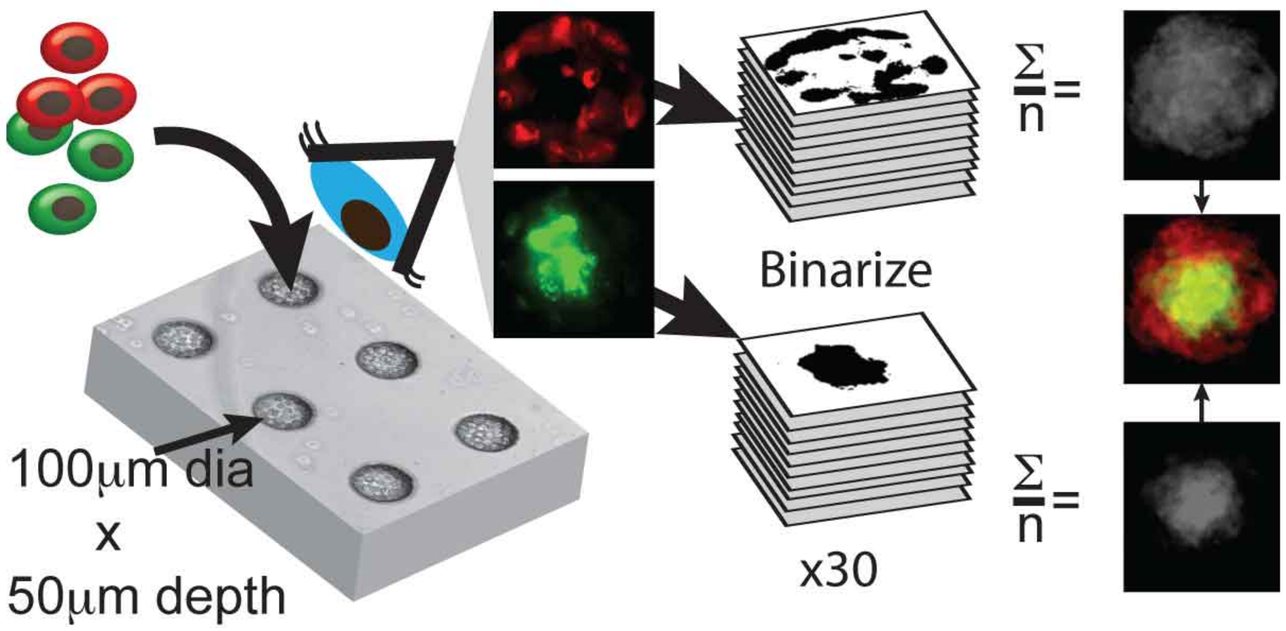
100μm dia
x
50μm depth
Binarize
x30
Σ
n

D

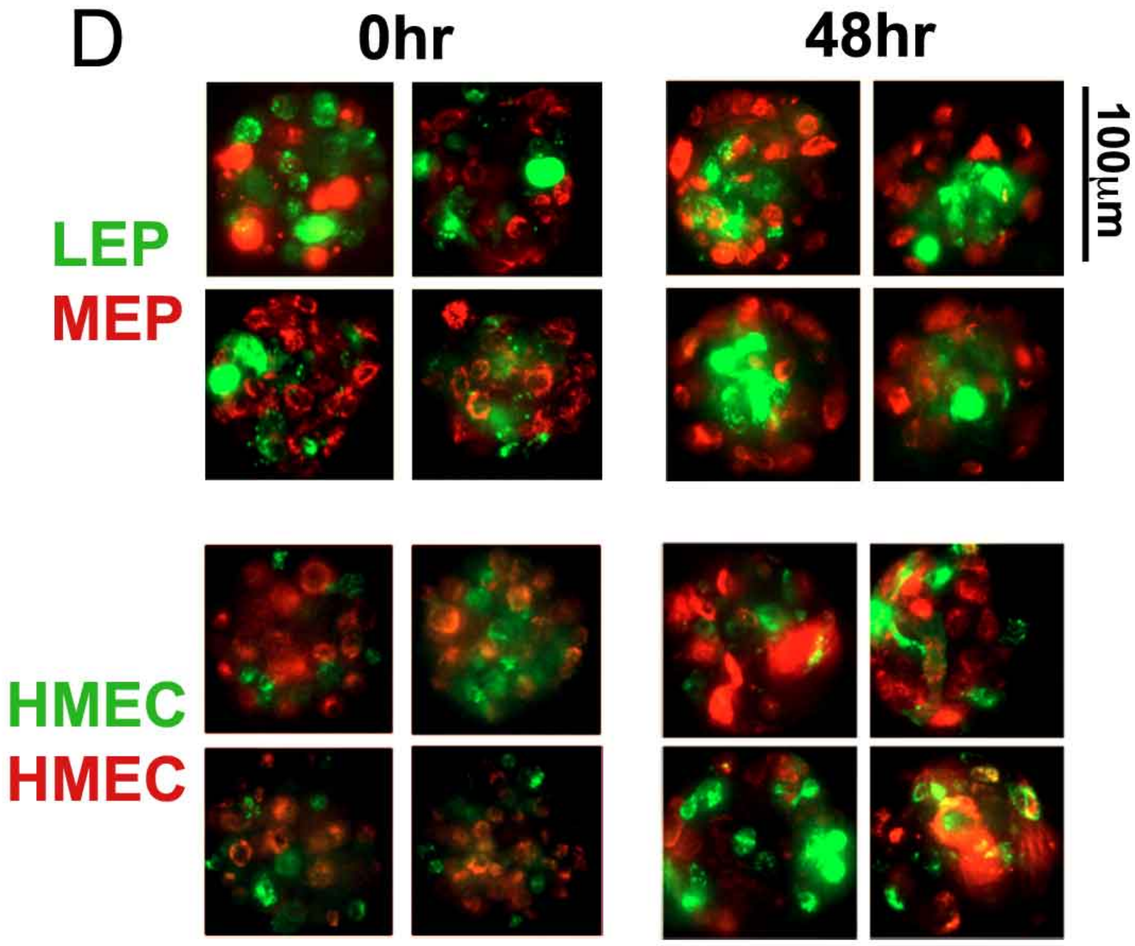
0hr
48hr
100μm
LEP
MEP
HMEC
HMEC

E

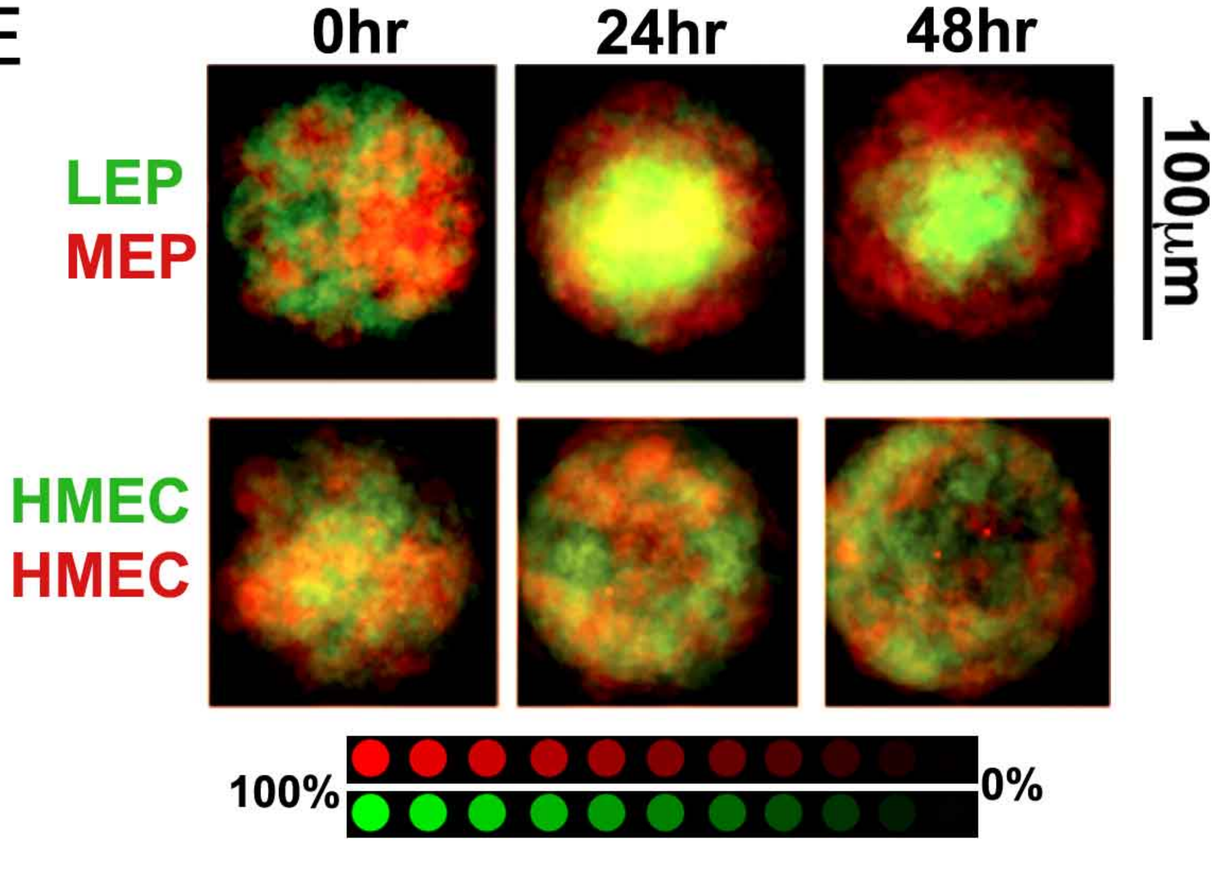
0hr
24hr
48hr
LEP
MEP
100μm
HMEC
HMEC
100%
0%

Chanson etal 2010 Figure 2

A

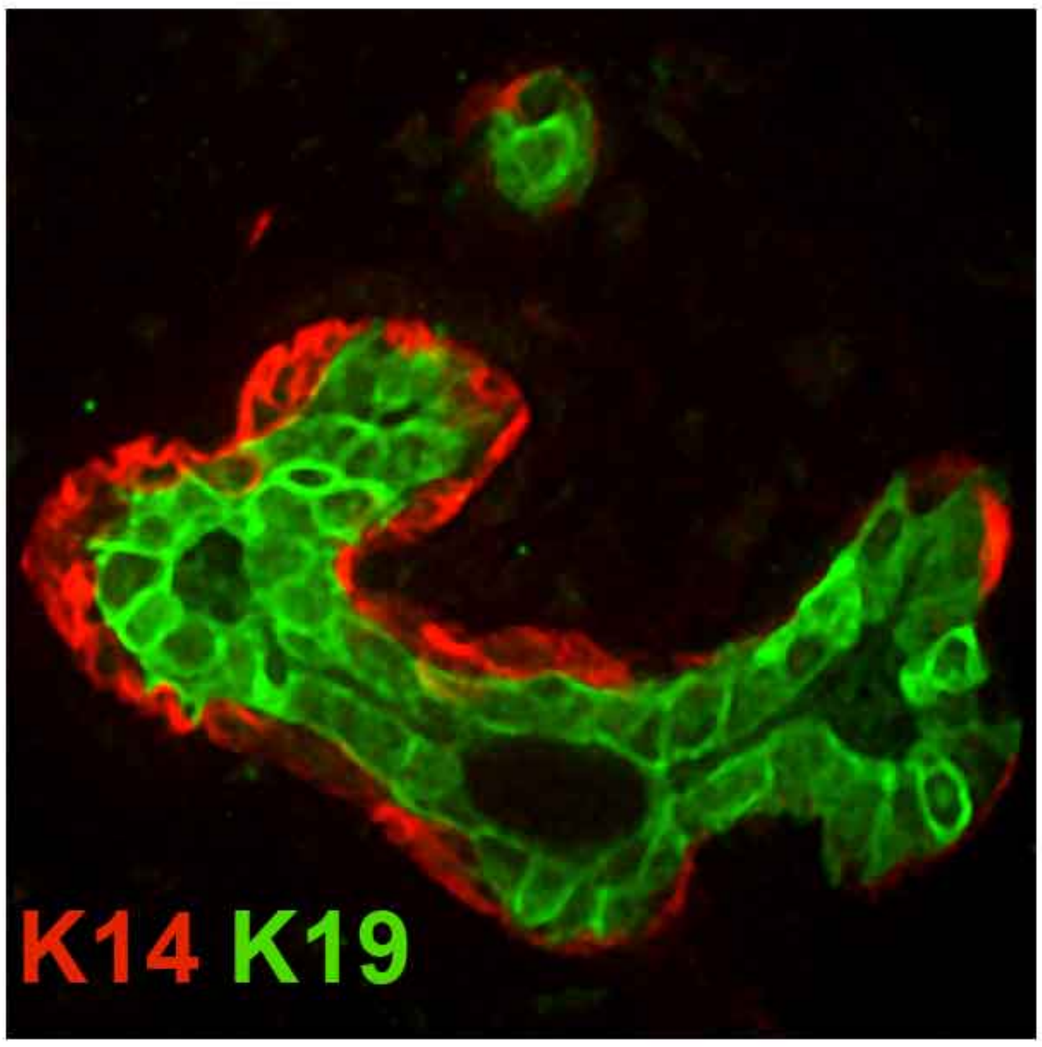

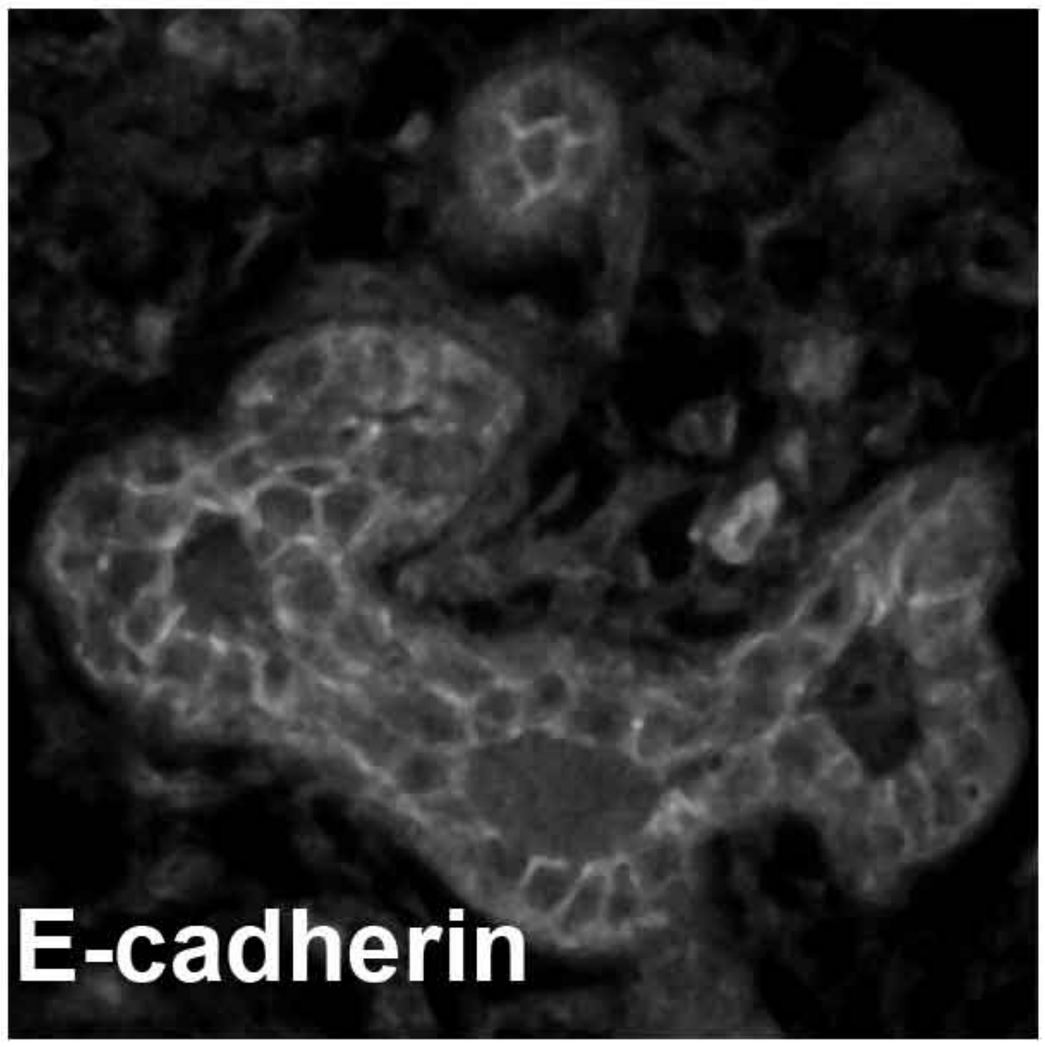

B

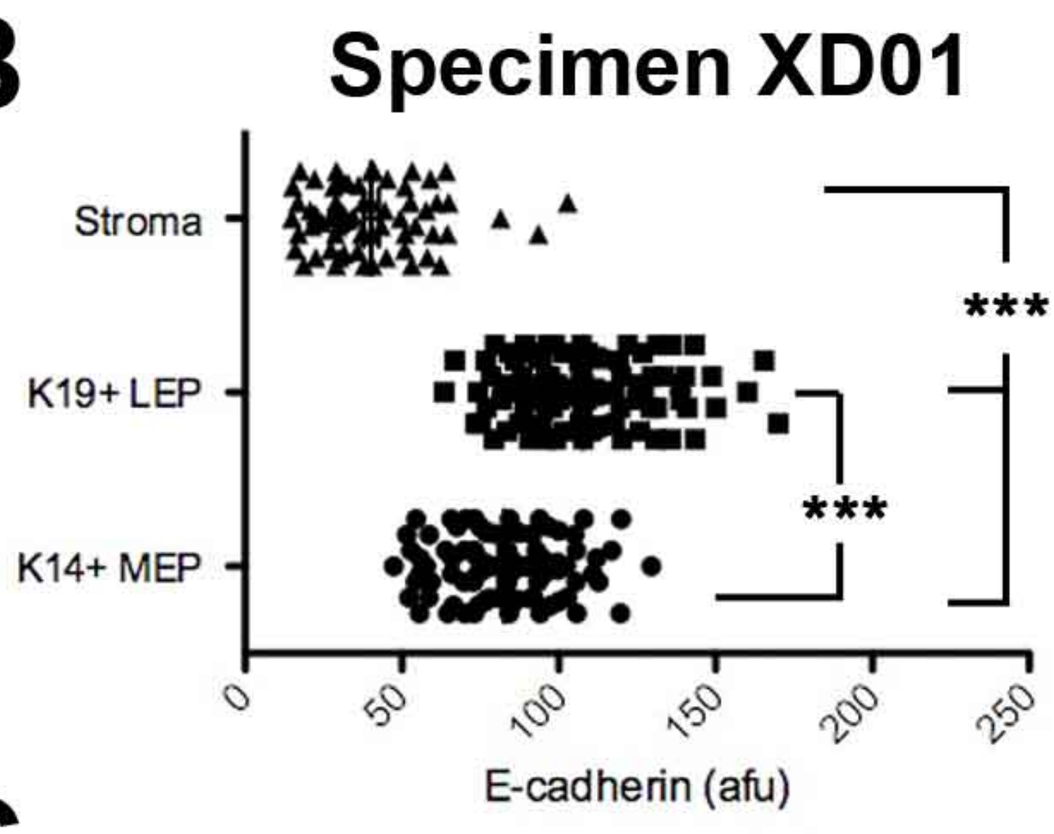

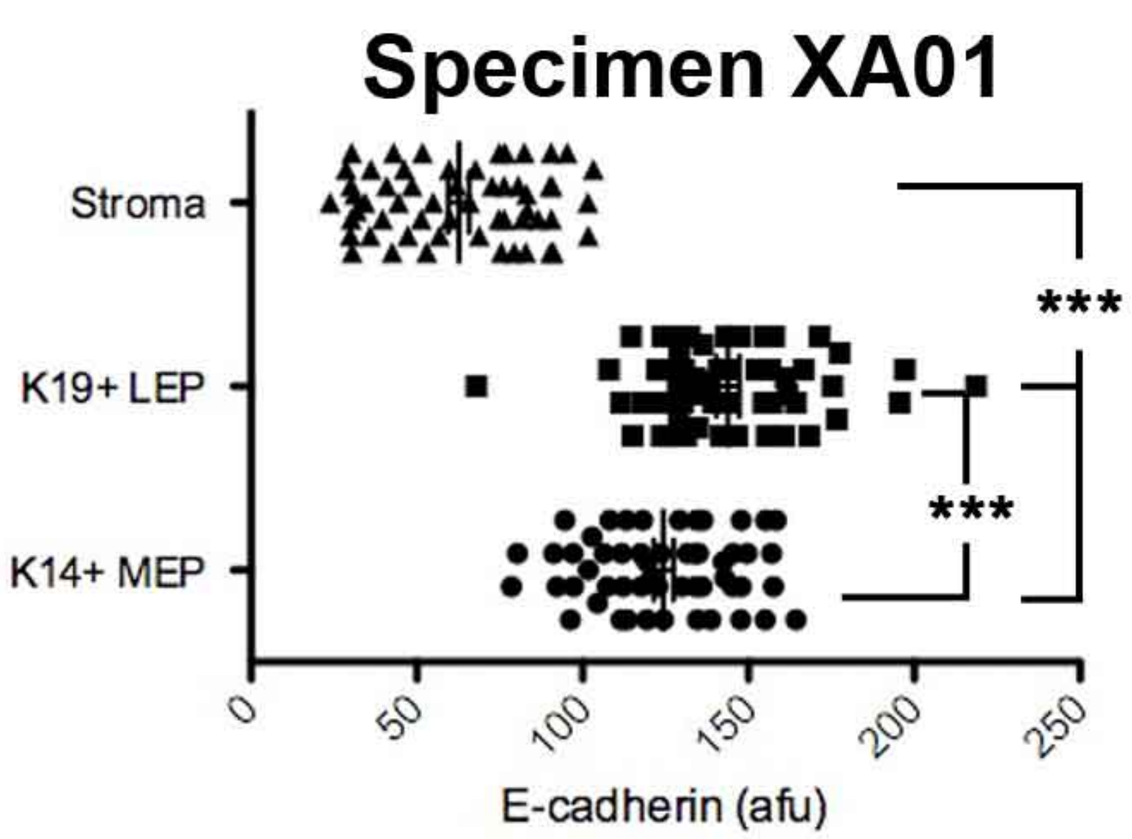

C

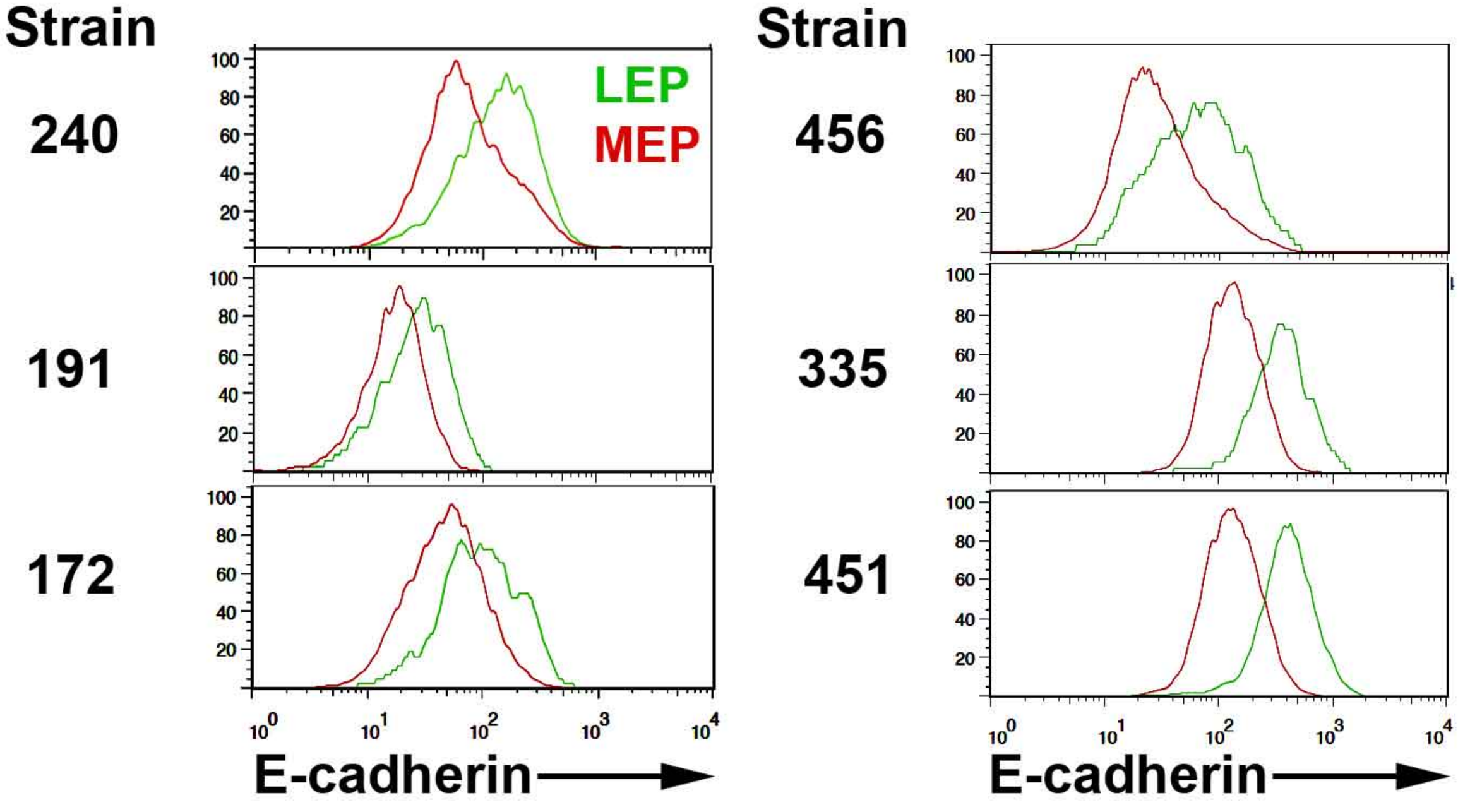

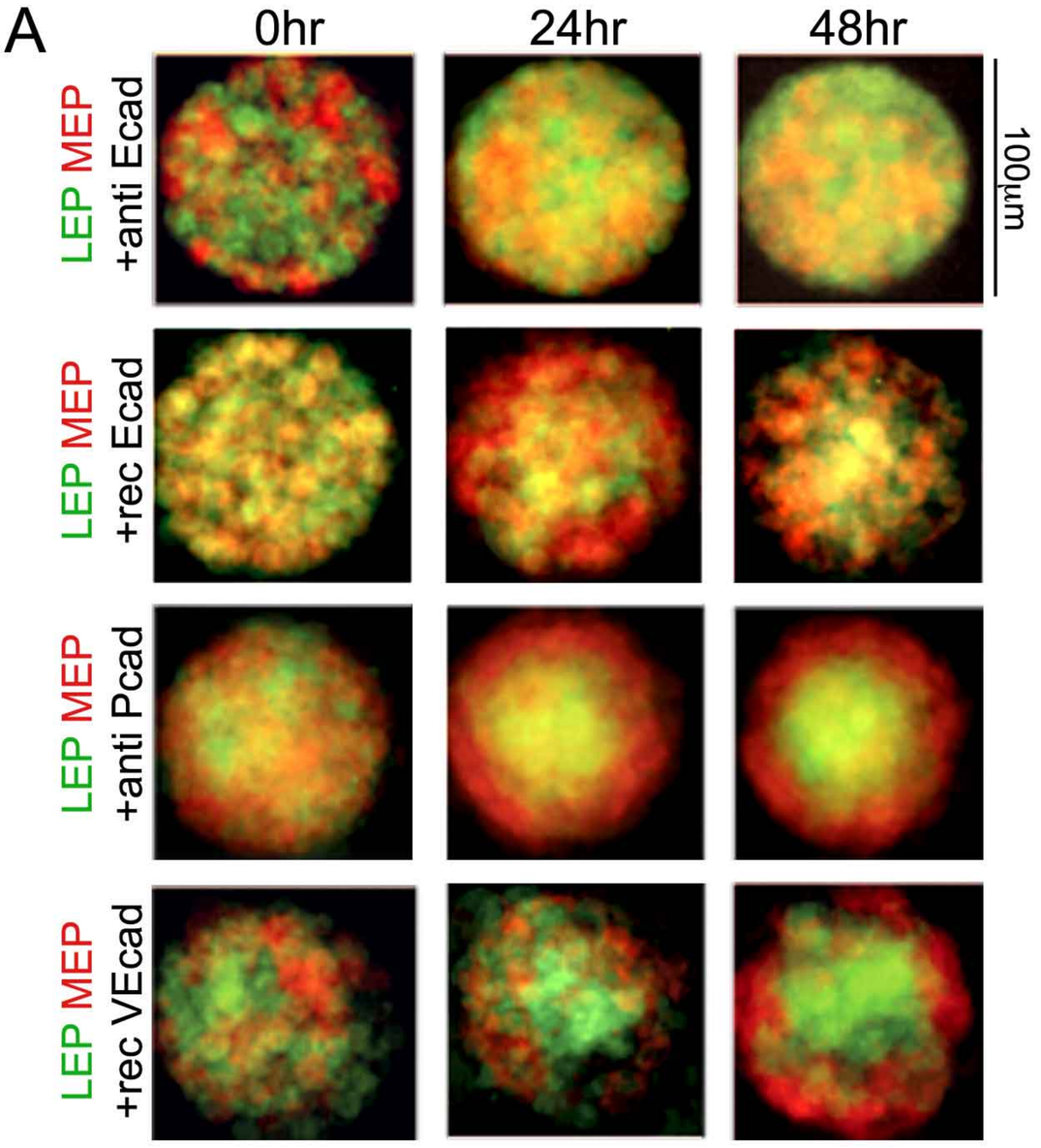
A
0hr
24hr
48hr
LEP MEP
+anti Ecad
LEP MEP
+rec Ecad
LEP MEP
+anti Pcad
LEP MEP
+rec VEcad
100μm

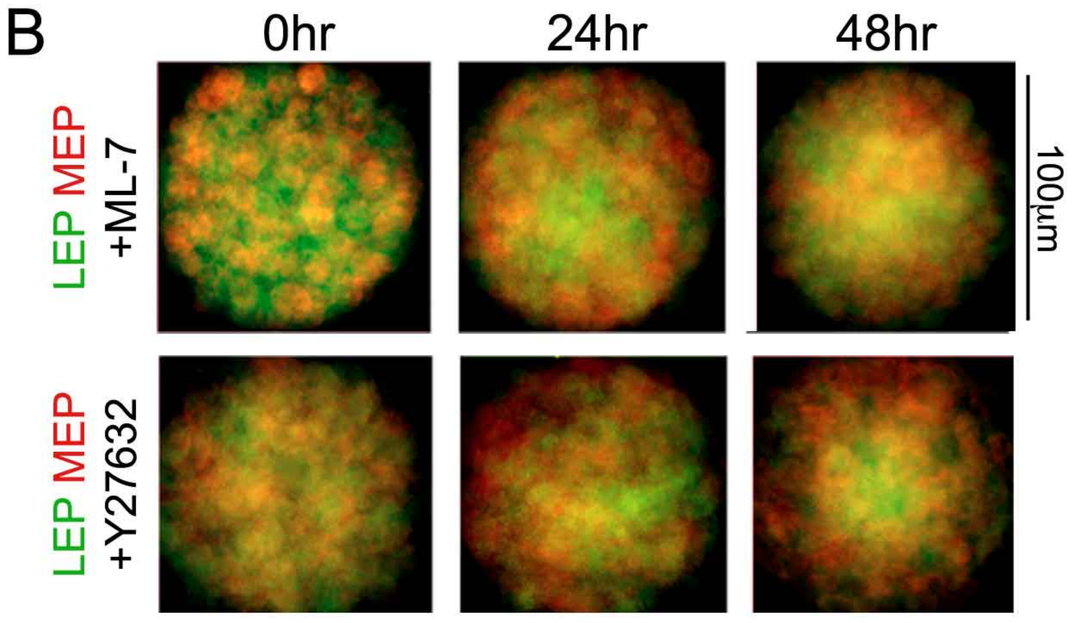
B
0hr
24hr
48hr
LEP MEP
+ML-7
LEP MEP
+Y27632
100μm

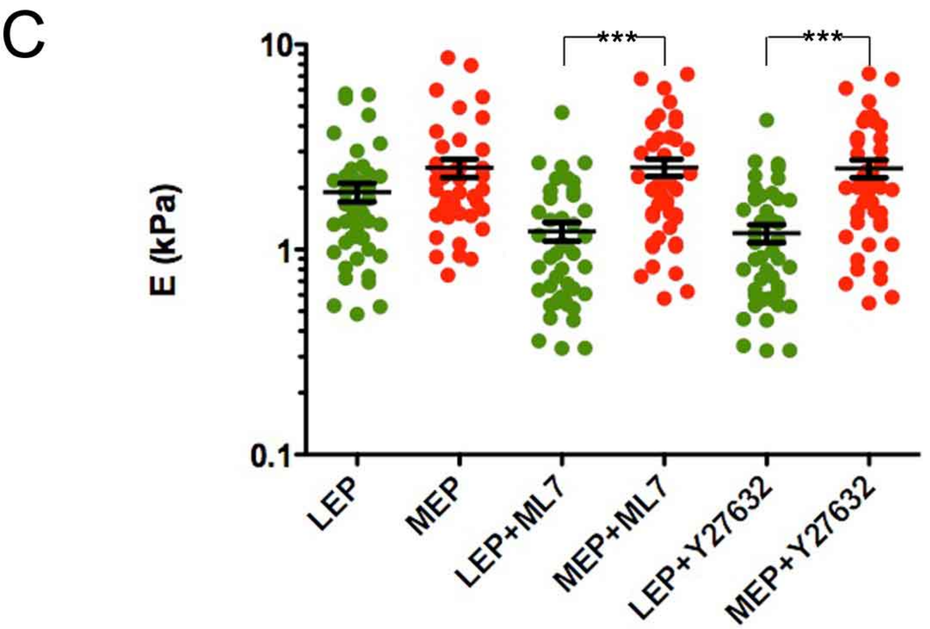
C
E (kPa)
10
1
0.1
***
***
LEP
MEP
LEP+ML7
MEP+ML7
LEP+Y27632
MEP+Y27632

A

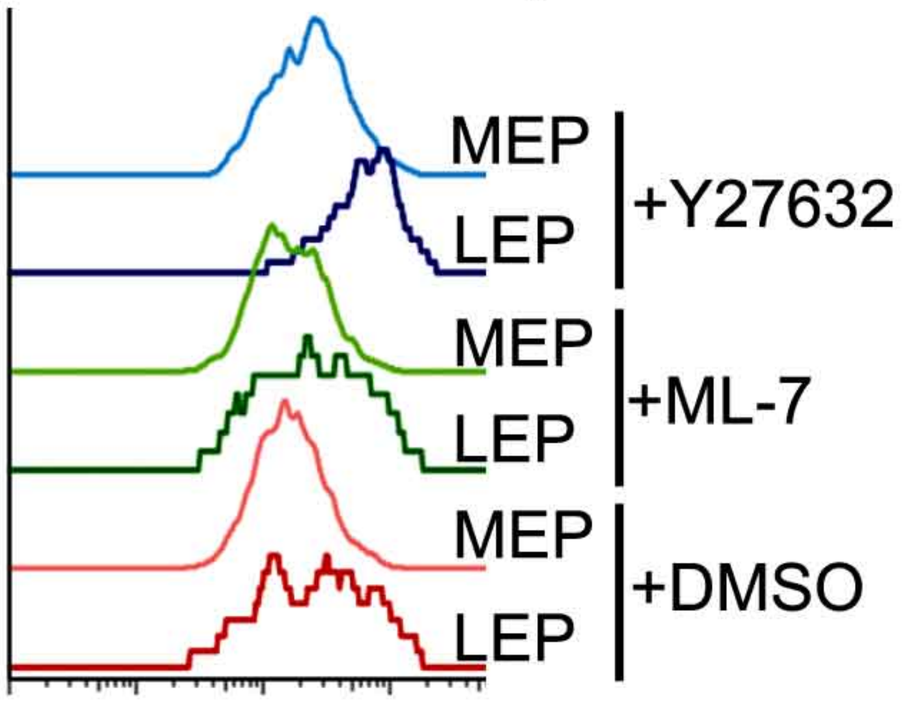
E-cadherin expression
MEP
LEP
+Y27632
MEP
LEP
+ML-7
MEP
LEP
+DMSO
E-cad expression

B

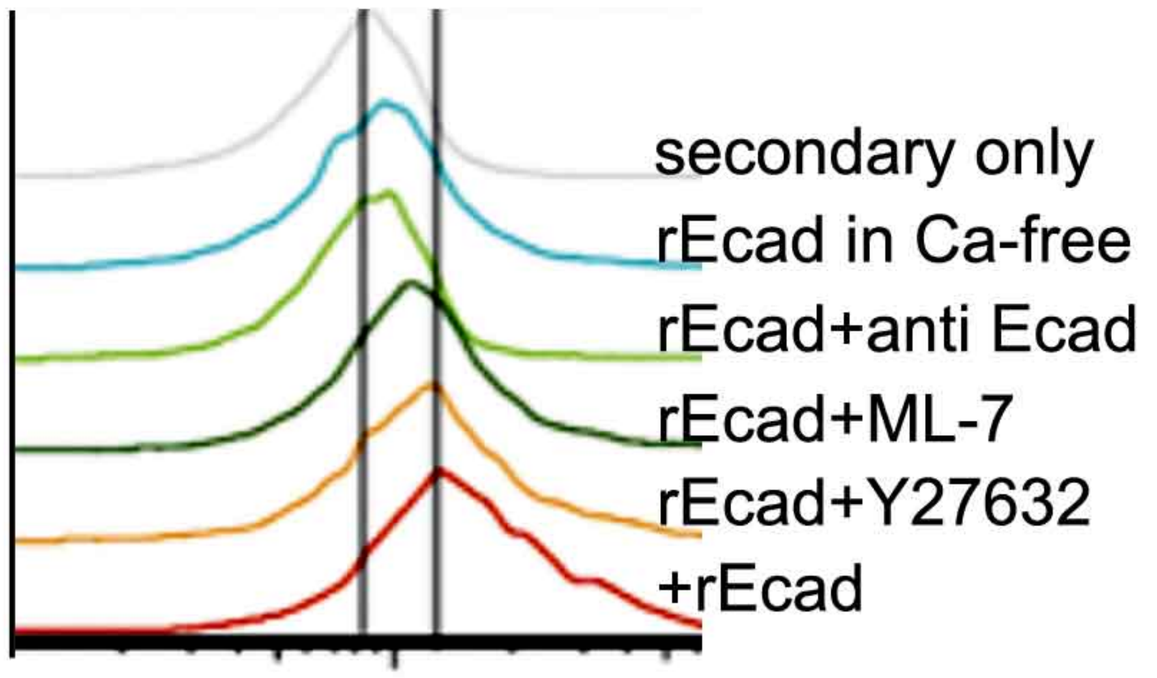
E-cadherin binding
secondary only
rEcad in Ca-free
rEcad+anti Ecad
rEcad+ML-7
rEcad+Y27632
+rEcad
rEcad binding

C

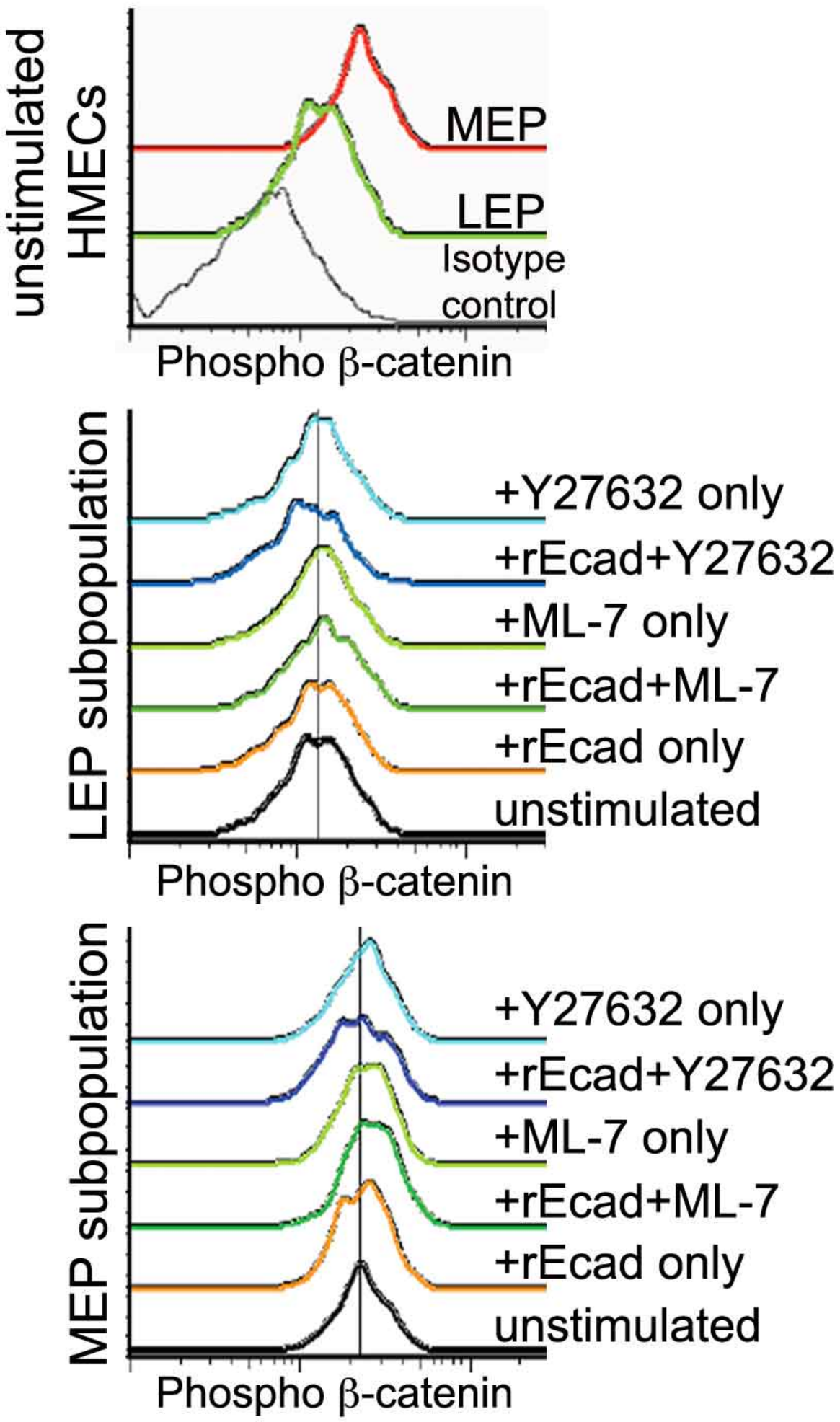
β-catenin phosphorylation
unstimulated HMECs
MEP
LEP
Isotype control
Phospho β-catenin
LEP subpopulation
+Y27632 only
+rEcad+Y27632
+ML-7 only
+rEcad+ML-7
+rEcad only
unstimulated
Phospho β-catenin
MEP subpopulation
+Y27632 only
+rEcad+Y27632
+ML-7 only
+rEcad+ML-7
+rEcad only
unstimulated
Phospho β-catenin

D

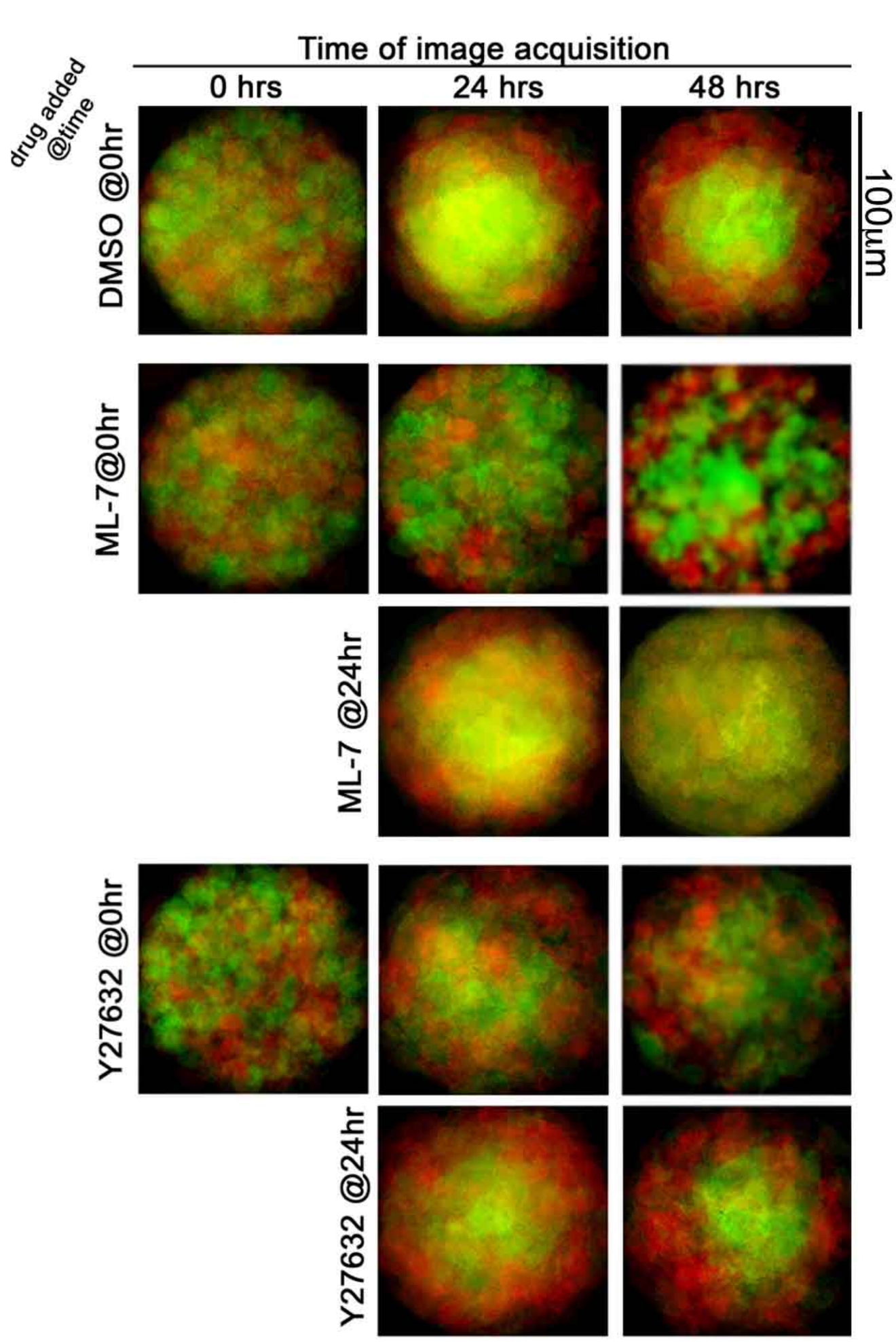
Self-organizing dynamics
Time of image acquisition
0 hrs
24 hrs
48 hrs
drug added @time
DMSO @0hr
100um
ML-7@0hr
ML-7 @24hr
Y27632 @0hr
Y27632 @24hr

Supplemental online material

Materials and methods

Cell culture – HMEC strains were established and maintained according to previously reported methods (*1, 2*). Finite lifespan pre-stasis HMEC were obtained from reduction mammoplasty tissue (strains 240, 191, 172, and 456) or from surgically resected non tumor areas of mastectomy tissue (strains 335P and 451P). Cells were initiated as organoids in primary culture in M85 or M87A and subjected to multiple partial trypsinizations as described. Cells were maintained in M87A medium, and used for assays at 4^{th} and 5^{th} passages; strain 240 was the only strain used for self-organizing, E-cadherin expression and binding assays, and phospho-beta-catenin assays.

Microwell self-organization assay - Micropatterned substrata were made according to Tan et al (*3*). Briefly, PDMS microwell arrays were formed by curing prepolymer with base : cure ratio of 10 : 1 (Sylguard) against a prepatterned master. The arrays of wells were peeled away, cut into 1cm^2 pieces that were affixed with a few mL of uncured PDMS to the bottom of a 24-well plate with good optical properties (Mitek). Plates were UV oxidized for 7 min (UVO-Cleaner 42, Jelight Co.), blocked with 2mg/mL BSA (Sigma) for 1 hour, and rinsed with PBS and M87A. Flow cytometry sorted HMEC were stained with CM-DiI, SP-DiOC_{18}(3), or DiIC_{18}(5)-DS (Invitrogen), used at 1:1000 in PBS for 5 minutes at 37C followed by 15 minutes at 4C. Cells were extensively washed with media following staining. Dye-stained cells HMEC were mixed at ratios of 1:1 (LEP:MEP), or 1:1 (randomly stained green:red HMEC cultures), and resuspended in M87A at one million cells per mL. HMEC were then introduced into the wells and allowed to load for 30-60 minutes, excess cells were washed away with media. All self-organizing experiments were conducted with HMEC strain 240. Inhibitors were added to the cell suspensions just before they were added to wells, and more was added to the media following the washing away of cells that were not inside the wells: Anti-E-cadherin at 100mg/mL (Invitrogen, clone HECD-1), anti P-cadherin 100mg/mL (Abcam, clone NCC-CAD-299), rhE-cadherin-Fc (rEcad) at 100mg/mL (R&D Systems), rhVE-cadherin at 100mg/mL (R&D Systems), Y27632 at 10^{-5}M (Calbiochem), or ML-7 at $3x10^{-6}$M (Calbiochem). HMEC were imaged at 0, 24, or 48 hours with a spinning disc confocal microscope (Carl Zeiss). Red and green fluorescence channels in images taken of thirty wells from each condition at each time point were binarized using the Threshold function, merged into a Z-stack, then averaged (NIH ImageJ). Gray-scaled average images corresponding to LEP and MEP were merged into a single image with red or green look up tables applied to each average image.

Flow cytometry sorting and assays– HMEC at 4th or 5th were trypsinized and resuspended in their media. For enrichment of LEP and MEP images, anti-CD227-FITC (BD, clone HMPV) or anti-CD10-PE (BioLegend, clone HI10a) were added to the media at 1:50 for 25minutes on ice, washed in PBS and sorted on a FACS Vantage DIVA (BD) into their own media.
E-cadherin expression was measured on LEP and MEP by addition of anti-E-cadherin-A647 (Biolegend) to the above cocktail at 1:50. To determine effects of inhibitors, Y27632 at 10^{-5}M (Calbiochem) or ML-7 at $3x10^{-6}$M (Calbiochem) were added to HMEC media 6 hours at 37C and 5% CO_2 before measurement of E-cadherin.

To measure the ability of rEcad to bind to HMEC in presence of inhibitors, cells were suspended in their media in Falcon tubes, to prevent adhesion to a culture surface, in presence of Y27632 at 10^{-5}M (Calbiochem), ML-7 at $3x10^{-6}$M (Calbiochem), or anti-E-cadherin at 100mg/mL (Invitrogen, clone HECD-1), or in calcium-free medium for 6 hours at 37C and 5% CO_2. rEcad was added at 100mg/mL in their own media for 1 hour on ice, washed with media, then incubated with anti-human IgG-A633 (1:500, Invitrogen) in their own media.

To measure phospho-beta catenin levels, cells were suspended in their media in Falcon tubes, to prevent adhesion to a culture surface, in presence of Y27632 at 10^{-5}M (Sigma) or ML-7 at $3x10^{-6}$M (Calbiochem), with and without rEcad at 100mg/mL (R&D systems) for 6 hours at 37C and 5% CO_2. Cells were fixed with 1.5% EM-grade paraformadahyde in PBS for 10 minutes at room temperature, pelleted in a centrifuge, then resuspended in 100% methanol for 30 minutes at 4C. Cell were pelleted and resuspended in PBS/2/%BSA and incubated on ice with anti-phospho-b-catenin-PE (1:100, BD) for 30 minutes.

AFM stiffness measurements - Once samples were equilibrated to 25°C, cell deformity measurements were performed and stiffnesses calculated as previously described (*4*). Briefly, a Bioscope Catalyst AFM (Veeco, Santa Barbara, Ca) was mounted onto an inverted microscope. Using a low spring constant cantilever (k = 0.03 N/m) (Veeco), the central region, excluding the nucleus, of each cell was initially contacted. Afterwards, a cantilever deflection versus sample height curve was gathered under moderate deflection (~3μm). An apparent stiffness was calculated using a custom Matlab (Mathworks, Natick, MA) script assuming a Hertz model. The resulting data was plotted using Prism(GraphPad Software, La Jolla, CA) (n = 45).

Immunofluorescence staining - FACS sorted HMEC were allowed to adhere to methanol-cleaned coverslips for 2 hours. Adherent cells were fixed in methanol:acetone (1:1) at -20C for 15 minutes, blocked with PBS/5% normal goat serum/0.1% Triton X-100, and incubated with

anti-K14 (1:1000, Covance, polyclonal) and anti-K19 (1:20, Developmental Studies Hybridoma Bank, clone Troma-III) overnight at 4C. Goat anti-rabbit-A568 and goat anti-rat-A488 secondaries (1:500, Invitrogen), and Hoechst 3342 (1:1000, Sigma) were added for 2 hours at room temp. Cells were imaged with an spinning disc confocal microscope (Carl Zeiss). Sections of normal human breast tissue, formaldehyde-fixed and paraffin embedded (FFPE), 4 micron thick, sections affixed to slides, were purchased from ProSci (http://www.prosci-inc.com/). Slides were baked at 55C for one hour to fix the tissue to the slide and to remove much of the paraffin. Complete deparaffinization was done according to protocol published on their website by Abcam. Antigen retrieval was done by following the Citrate buffer, pH6.0 based protocol published on Abcam website. Slides were not allowed to dry out after deparaffinization, and were stored in PBS at 4*C if not stained immediately. Prior to reaction with primary antibodies, the slides were blocked for one hour at room temp or overnight at 4*C in NGS blocking buffer: 5% normal goat serum (NGS), 0.001%azide, 0.1% Triton, PBS. The unconjugated primary antibody recognizing human cytokeratin (K) 19 was diluted 1:100 in NGS block buffer prior to incubation with the slides in a coldroom on a rocker platform overnight, followed by 3 consecutive 10min washes in PBS at ambient temperature. Secondary antibodies (Goat-anti-mouse-Alexa 568 were diluted 1:500 in PBS and incubated with the slides for one hour at ambient temperature on a slow rocking platform, followed by 3 washes in PBS, 10minutes each. The conjugated antibodies against K14 (Alexa633) and against E-cadherin (Alexa488) were then diluted 1:100 in NGS blocking buffer and incubated with the slides overnight in a coldroom on a rocker platform, followed by 3 washes in PBS, 10minutes each. DAPI diluted 1:4000 in PBS was added to the slides for 5 minutes, then rinsed with PBS and destained overnight in PBS in the cold room. The following day slides were overlaid with Fluoromount and a #1 coverslip, and allowed to dry in the dark at ambient temperature overnight before sealing with ordinary clear nail polish. Imaging was accomplished on a Zeiss 510 spinning disc confocal microscope. For each area of interest, 5 focal planes were imaged of approximately 2 micron vertical separation. Images were processed using Image J software. K14 (Covance) (1-800-922-2226) purified rabbit polyclonal antisera MK14 (AF 64), catalog # PRB-155P, supplied in PBS, 0.03% Thimerosal – conjugated with Alexa 633 fluor following protocol from Molecular Probes. Briefly, Alexa 633, 1 mg, was purchased from Invitrogen/Molecular Probes, resuspended at 5 mg/ml in acetonitrile and used at 10-fold molar excess to the IgG. Excess Alexa-633 was aliquoted and rotovapped to dryness then stored in dark at -20C. K19 Abcam ab7754 (mouse MAb IgG2A) use at 1:100, E-cadherin Ab, Alexa 488 conjugated #3199 from Cell Signaling. Specificity of anti-E-cadherin was determined using recombinant E-cadherin peptide conjugated to Fc fragment of human IgG (blocking) from R&D Systems (catalog #648-EC) used at 1:5 dilution, equivalent to 50 ug/ml.

Statistics - E-cadherin image analysis and atomic force microscopy analysis were analyzed using one-way ANOVA followed by the Kruskal-Wallis post-test and Dunn's test for multiple comparisons, using a 95% confidence interval.

1. J. C. Garbe *et al*., *Cancer Res* **69**, 7557 (Oct 1, 2009).
2. M. R. Stampfer, J. C. Bartley, *Proc Natl Acad Sci U S A* **82**, 2394 (Apr, 1985).
3. J. L. Tan, W. Liu, C. M. Nelson, S. Raghavan, C. S. Chen, *Tissue Eng* **10**, 865 (May-Jun, 2004).
4. J. Alcaraz *et al*., *EMBO J* **27**, 2829 (Nov 5, 2008).

DISCLAIMER